Hindawi Publishing Corporation
Advances in Condensed Matter Physics
Volume 2013, Article ID 328402, 9 pages
http://dx.doi.org/10.1155/2013/328402

Research Article

Near-Zero-Refractive-Index Structure at Optical Frequencies

Hassan S. Ashour[1,2]

[1] *Department of Physics, Al-Azhar University, Gaza, Palestine*
[2] *Department of Physics, University of Dayton, Dayton, OH 45469, USA*

Correspondence should be addressed to Hassan S. Ashour; hashour@alazhar.edu.ps

Received 31 May 2013; Accepted 8 September 2013

Academic Editor: Rosa Lukaszew

We have used a new class of left-handed materials, which uses 3D nanospheres distributed in loops in the dielectric host material. These 3D nanospheres loops give rise to negative effective permeability and permeability at Terahertz (optical) frequencies. The modal dispersion relation for Terahertz TE surface waves has been derived for a slab waveguide constructed from a dielectric material slab sandwiched between two thick layers of Terahertz left-handed material (LHM). The modal dispersion relation and the power flow were numerically solved for a given set of parameters: dielectric slab thickness, the operating frequency, mode order, and the power flow and extinction in the structure. The real part of the effective refractive index exhibits near-zero values, with small extinction coefficient values. Besides that, the power flow in the dielectric core increased with slab thickness increase and the power attenuation decreased with thickness increase.

1. Introduction

In 1986, Victor G. Veselago, in his pioneer paper, proposed the electromagnetic propagation in an isotropic medium with negative dielectric permittivity $\varepsilon(\omega) < 0$ and negative permeability $\mu(\omega) < 0$ [1]. Prior year 2000 no such materials hold these characteristics and index of refraction with negative values. In the year 2000 a group of researchers at the University of San Diego were able to synthesize an artificial dielectric medium (metamaterial). They were able to demonstrate that those materials exhibit both negative dielectric permittivity and magnetic permeability simultaneously over a certain range of frequencies (in Gigahertz) [2, 3]. They impeded split ring resonators (SRRs), which have many shapes and structures based on the range of the frequencies in interest [4–6], to induce desired magnetic effects to have negative effective permeability in the host material. Besides that, they embedded arrays of long metallic nanowires (ALMWs) to induce negative effective permittivity [7]. The early negative index of refraction has been realized in microwave and infrared. Since this realization, metamaterials gained momentum and the attention of many researchers in physics and engineering realm. It is used in fabricating transmission lines [8, 9], microstrip resonators [10], couplers [11], resonators [12], and antennas [13]. Besides that, subdiffraction imaging [14], invisibility cloaks [15], chemical and biomolecular sensing [16], and communication and information processing [17] are some of the applications that have generated enormous interest in metamaterials over a relatively short time span. However, there are many applications that demand class of metamaterials, which operate at optical frequency, that is, integrated metamaterial modulator on optical fiber [18, 19], which was the driving force to realize such metamaterials that operate at optical frequencies. Alù et al. [20] had proposed metamaterials structure which operate at optical frequencies. They used spherical sliver nanoparticles embedded in dielectric host material. Other researchers have incorporated nanowires [21], and other classes of nanospheres to achieve the negative index of refraction at optical frequencies was employed using semiconductor and metal's nanoparticles [22]. Chaturvedi demonstrated a novel class of metamaterials that can be used in super-lensing and with fiber-integrated modulator for telecommunication applications [23]. Most recently, interest has shifted towards the realization of materials that exhibit zero or near-zero refractive index [24–27]. In this class of

materials a zero phase delay is achievable, which implies that light enters a state of quasi-infinite phase velocity and infinite wavelength [28]. Thus, every point within the metamaterial experiences a quasi-uniform phase, as though all the dipoles inside the metamaterial are oscillating in unison [28]. Thus, the shape of the wavefronts leaving the metamaterial depends solely on the shape of the exit surfaces of the metamaterial, which provides high flexibility in the design of phase patterns [28]. Alù et al. and others have [26, 29, 30] investigated the response of epsilon-near-zero metamaterials and plasmonic materials to electromagnetic source excitation, and in 2011 zero-refractive-index metamaterial at IR wavelength was engineered at Columbia University [26]. Low values of permittivity and permeability gave rise to a new class of metamaterials, which is near-zero-index materials (NZIM). In the near-zero-index regime, the electromagnetic field is static in the spatial domain (the phase difference between any two arbitrary points is equal to zero) while remaining dynamic in the time domain, thus allowing energy transport [28, 29]. Besides that, near-zero-index materials have potential applications such as microstrip technology [27, 31], beam self-collimation [32], and strong field enhancement [33]. Tiny values of the refractive index of near-zero-index materials can reshape electromagnetic phase fronts emitted by optical antennas [34] or, for highly directive antennas, transfer near-field phase information into the far-field. Perhaps the most important application of near-zero-index materials is in optical links in lumped nanophotonic circuits [35].

Dielectric layers acting as waveguide are well suited for use in integrated optics. These waveguides structures can be integrated with solid-state laser sources and with electronics that can process light signals [36]. These advancement and potentially important class of applications motivated us to seek for a structure that has two important features, namely, near-zero index of refraction at Terahertz frequency, and it is easy to fabricate with potential applications. This paper is organized as follow. In Section 2, we outline the Terahertz left-handed material using nanospheres inclusion in the host material. In Section 3, we derived the modal dispersion relation of the proposed structure, the power flow, and the confinement factor. In Section 4, we numerically solve the dispersion relation for several guiding layer thickness and for the certain range of frequencies. Section 5 is solely devoted to the conclusions of this study.

2. Terahertz Left-Handed Material

In 2006, Alù et al. [20] had proposed a nonconventional class of left-handed material. The new class is unlike the usual left-handed material which depends on split ring resonator, SRR, and embedded parallel nanowires or nanoplates in the host material. They achieved left-handed properties at optical frequencies, in Terahertz, by inserting a circular array of equispaced sliver nanospheres in a host dielectric material as in Figure 1. The new design idea depends on the collective resonance of a circular pattern array of plasmonic nanoparticles. In this ring, the plasmonic resonant feature of every nanoparticle induces a circulating "displacement" current around this loop [20]. Unlike the case of the conventional metallic loops or SRRs at the microwave frequencies, plasmonic resonant frequency of the nanoparticle is the main determining factor for this resonance to happen [20].

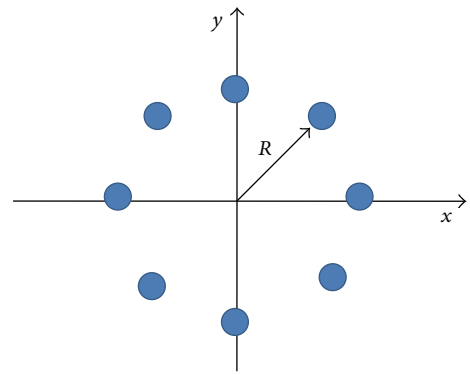

Figure 1: A circular array with $N = 8$ equispaced nanospheres in the x-y, with circle's radius R.

The magnetic permeability constant of the terahertz left-handed material is given by [20, 37–40]

$$\mu_{\text{eff}}(\omega) = \mu_0 \left(1 + \frac{1}{N\left[\alpha_{mm}^{-1} + i\left(k_b^3\right)\right] - 1/3}\right), \tag{1}$$

where

$$\alpha_{mm}^{-1} = \frac{4\varepsilon_b}{Nk_b^2R^2}\alpha - i\left(\frac{k_b^3}{6\pi} - \frac{2k_b}{3\pi NR^2}\right) + \frac{1}{16\pi Nk_b^2R^5}\sum_{l\neq n}^{N}\frac{3+\cos\left[2\pi\left(l-n\right)/N\right]}{\sin\left[\pi\left(l-n\right)/N\right]^3}, \tag{2}$$

where α_{mm} is the magnetic polarizability of the nanoring, N is number of the identical nanospheres with radius a, λ_b is the wave length in the background medium, R is the circle's radius, ε_b is background material dielectric constant, $k_b = \omega\sqrt{\varepsilon_b\mu_0}$ is the background wave number, $n = 1, 2, \ldots N$, and α is given by

$$\alpha = \left[\left(4\pi\varepsilon_b a^3\frac{\varepsilon-\varepsilon_b}{\varepsilon+2\varepsilon_b}\right)^{-1} - i\frac{k_b^3}{6\pi\varepsilon_b}\right]^{-1}, \tag{3}$$

where ε is the permittivity of a single isolated nano-sphere, and the effective permittivity is given by

$$\varepsilon_{\text{eff}}(\omega) = \varepsilon_0\left(1 + \frac{1}{\varepsilon_0 N_d^{-1}\left[\alpha_{ee}^{-1} + i\left(k_0^3/6\pi\varepsilon\right)\right] - 1/3}\right), \tag{4}$$

where N_d is number density of the loop inclusions per unit volume, α_{ee} is electric polarizability of the loop, and $k_0 = \omega\sqrt{\varepsilon_0\mu_0}$ is the background wave number. Equations (1) through (4) are obtained in the limit $k_b \ll 1$ and $a \ll$

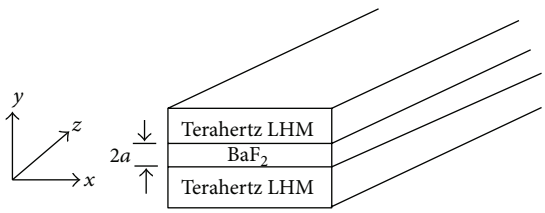

Figure 2: Geometrical structure of the slab waveguide. The upper and lower layers (cladding and substrate) are made from Terahertz left-handed metamaterial, and the core is dielectric material (BaF_2 glass).

$R \ll \lambda_b$. The material exhibited both negative effective permeability and negative permittivity, in the frequency range from 630 THz to 634 THz, at optical frequency for the following parameters: $R = 40\,\text{nm}$, $a = 16\,\text{nm}$, $N = 6$, $N_d = (108\,\text{nm})^{-3}$, and $\varepsilon_b = 2.2\varepsilon_0$. These values would give rise to both effective permittivity and permeability which have negative real parts simultaneously at 630–634 terahertz.

3. Theory

3.1. TE Modes Dispersion Relation. We briefly outline the derivation of the dispersion relation for TE surface waves in the proposed waveguide structure [41, 42]. The dispersion relation for TE modes propagation in the z-axis with complex propagation wave constant β is represented in the form $e^{i(\omega t-\beta z)}$, where $\beta = k/k_0$, k is the effective wave index, and k_0 is the free space wave number which equals ω/c, where c is the velocity of light and ω is the applied angular frequency. Figure 2 shows the geometry and coordinates of the structure under investigation. The structure, shown in Figure 2, is an isotropic dielectric material core, $-a < y < a$, surrounded by thick cladding and substrate layers of Terahertz left-handed material. The electromagnetic field components are

$$\widetilde{E} = E(x,y)\exp(i(\omega t-\beta z)),$$
$$\widetilde{H} = H(x,y)\exp(i(\omega t-\beta z)). \tag{5}$$

Substitution of (5) into Maxwell's equation yields the following linear differential equations for the core and cladding, respectively, which are given by

$$\frac{\partial^2 E_{y1}}{\partial x^2} + \kappa^2 E_{y1} = 0, \tag{6}$$

$$\frac{\partial^2 E_{y2,3}}{\partial x^2} - \sigma^2 E_{y2,3} = 0, \tag{7}$$

where $\kappa^2 = \varepsilon_r(\omega)k_0^2 - \beta^2$ and $\sigma^2 = \beta^2 - \varepsilon_{\text{eff}}(\omega)\mu_{\text{eff}}(\omega)k_0^2$ are the wavenumbers in the core and cladding, respectively, where E_{y1} is the electric field in the guiding core and $\varepsilon_r(\omega)$ is the frequency-dependent electric permittivity, which can be obtained from Sellmeier dispersion relationship, which is given by [43]

$$\varepsilon(\lambda) = 1 + \frac{A_1\lambda^2}{\lambda^2-\lambda_1^2} + \frac{A_2\lambda^2}{\lambda^2-\lambda_2^2} + \frac{A_3\lambda^2}{\lambda^2-\lambda_3^2} + \cdots, \tag{8}$$

where λ_i is a constant and $A_1, A_2, A_3, \lambda_1, \lambda_2$, and λ_3 are called Sellmeier coefficients and have the following values for BaF_2 glass:

$$A_1 = 0.63356, \quad A_2 = 0.506762, \quad A_3 = 3.8261,$$
$$\lambda_1 = 0.057789, \quad \lambda_2 = 0.109681, \quad \lambda_3 = 46.38642. \tag{9}$$

The magnetic field components are

$$H_x = -\frac{\beta}{\omega\mu_0\mu_r},$$
$$H_z = -\frac{i}{\omega\mu_0\mu_r}\frac{dE_y}{dx}. \tag{10}$$

We consider the slab waveguide with uniform refractive-index profile in the core. We use the fact that the guided electromagnetic fields are confined in the core and exponentially decay in the cladding; the electric field distribution in the core and cladding is

$$E_y(x > a) = A\cos(\kappa a - \phi)e^{-\sigma(x-a)}, \tag{11a}$$

$$E_y(-a \le x \le a) = A\cos(\kappa x - \phi), \tag{11b}$$

$$E_y(x < -a) = A\cos(\kappa a + \phi)e^{\sigma(x+a)}. \tag{11c}$$

The electric field components E_y in (11a), (11b), and (11c) are continuous at the interface between the core and the cladding at $\pm a$. Neglecting the terms independent of x, the boundary condition for H_z is treated by the continuity condition of dE_y/dx as

$$\frac{dE_y}{dx}(x > a) = -\sigma A\cos(\kappa a - \phi)e^{-\sigma(x-a)}, \tag{12a}$$

$$\frac{dE_y}{dx}(-a \le x \le a) = -\kappa A\sin(\kappa x - \phi), \tag{12b}$$

$$\frac{dE_y}{dx}(x < -a) = \sigma A\cos(\kappa a + \phi)e^{\sigma(x+a)}. \tag{12c}$$

From the condition that the dE_y/dx are continuous at $x = \pm a$, we obtain the following:

$$\kappa A\sin(\kappa a + \phi) = \sigma A\cos(\kappa a + \phi), \tag{13a}$$

$$\sigma A\cos(\kappa a - \phi) = \kappa A\sin(\kappa a - \phi). \tag{13b}$$

Eliminating A from (13a) and (13b) and then rearranging we have the dispersion relation for TE modes; that is,

$$u = \frac{m\pi}{2} + \tan^{-1}\left(\frac{w}{u}\right), \tag{14}$$

where $u = \kappa a$, $w = \sigma a$, and m is the order of the TE mode.

3.2. Confinement Factor. The power flow is the real part of the integral of the complex Poyting vector over the waveguide cross section, that is

$$\begin{aligned} P &= \int_0^1 dy \int_{-\infty}^{\infty} \frac{1}{2}\left(\mathbf{E}\times\mathbf{H}^*\right)\cdot u_z dx, \\ &= \int_{-\infty}^{\infty}\left(E_x H_y^* - E_y H_x^*\right) dx. \end{aligned} \tag{15}$$

For TE wave we rewrite (15) using (10), as

$$P = \frac{\beta}{2\omega\mu_0\mu_{\text{eff}}}\int_{-\infty}^{\infty}\left|E_y\right|^2 dx. \tag{16}$$

Substituting (11a), (11b), and (11c) in (16), we have the power flow in each layer; that is,

$$P_{\text{core}} = \frac{\beta a A^2}{2\omega\mu_0\mu_{\text{eff}}}\left\{1 + \frac{\sin^2(u+\phi)}{2w} + \frac{\sin^2(u-\phi)}{2w}\right\}, \tag{17a}$$

$$P_{\text{clad}} = \frac{\beta a A^2}{2\omega\mu_0\mu_{\text{eff}}}\frac{\cos^2(u-\phi)}{2w}, \tag{17b}$$

$$P_{\text{sub}} = \frac{\beta a A^2}{2\omega\mu_0\mu_{\text{eff}}}\frac{\cos^2(u+\phi)}{2w}, \tag{17c}$$

where P_{core}, P_{clad}, and P_{sub} are the power in the core, cladding, core, and substrate. The power confinement factor in the core is defined by the power flow in the core to the total power flow in the waveguide. Thus, the power confinement factor can be calculated using (17a), (17b), and (17c); that is,

$$\Gamma = \frac{P_{\text{core}}}{P} = \frac{1 + \left(\sin^2(u+\phi)/2w\right) + \left(\sin^2(u-\phi)/2w\right)}{1 + (1/w)}, \tag{18}$$

where $P = P_{\text{core}} + P_{\text{clad}} + P_{\text{sub}}$ is the total power flow in the structure.

4. Numerical Results and Discussion

In this section, we explored the numerical solutions of the dispersion relation, (14), for TE_0. We found the effective wave index $\beta = n - i\gamma$ as a function of the electromagnetic wave at Terahertz frequency spectrum that lies between 630 and 634 Terahertz for a set of dielectric core thicknesses ($t = 30$, 40, 50, and 60 nm). Moreover, the power confinement factor and power attenuation were investigated for this waveguide structure. The parameters of the Terahertz LHM have been adjusted to have negative effective permittivity and negative effective permeability over the previously mentioned frequency spectrum; these parameters are given in Section 2. In Figure 3, we plotted the real part of the effective refractive index, n, versus the allowed frequency range at different dielectric core thicknesses, with dielectric constant for BaF_2 glass calculated using (7). Figures 3(a) to 3(d) shows the real part of the effective refractive index, n, for a set of core's thickness of this structure. The real refractive index is almost zero over the specified frequency spectrum. In Figure 3(a), for example, at $t = 30$ nm, the real part of the effective refractive index decreases with frequency increase with negative slope, which means the waveguide behaves like a left-handed material. The slope of the dispersion relation represents the group velocity [44, 45]. When the slope has a positive gradient this means that the group velocity is positive, and the structure behaves like RHM (right-handed material). This behavior continues with core's thickness 40 nm (Figure 3(b)). In Figures 3(c) and 3(d), the behavior starts to change for the thicknesses 50 nm and 60 nm; the structure behaves like left-handed material and then flips and behaves like a right-handed material. The common feature for these curves is that the real part of the effective refractive index in close to zero, with small variation across the allowed frequency spectrum.

In Figure 4, we plot the imaginary part of the effective refractive index, which is called the extinction (or absorption) coefficient, γ, of the structure versus the allowed frequency range. It can be noticed that the values of the extinction coefficient are small and decrease with the cores thickness increase. Moreover, small values of the extinction coefficient indicate that the structure is relatively transparent. At $t = 30$ nm (the dashed curve in Figure 4) the extinction coefficient decreases with frequency increase and dips down at almost $f = 632$ THz, and then it increases. This happens for almost all the core's thicknesses investigated in this paper, with small and negative extinction coefficient values.

In Figure 5, we plot the power confinement factor (18) versus the allowed frequency range for different core's thicknesses. Figure 5 shows that the power confinement factor gets higher values when the core thickness increases, which means we have better power confinement in the core when the core thickness increases. This implies the structure guides the optical power through the core more than wasting it in the cladding and substrate.

In Figure 6, we plotted the power attenuation (the imaginary part of (16)) versus frequency for different slab thicknesses. The power attenuation increases with dielectric core thickness increase; more power guidance leads to more power attenuation in the core, as concluded from Figure 5. In Figure 6, at lower frequencies the power attenuation is low and increases with frequency and thickness increase and peaks to the maximum at $f = 632$ THz.

In Figure 7(a), we explored the modal dispersion in the structure TE_m, $m = 0, 1, 2, 3$, for core's thickness 40 nm.

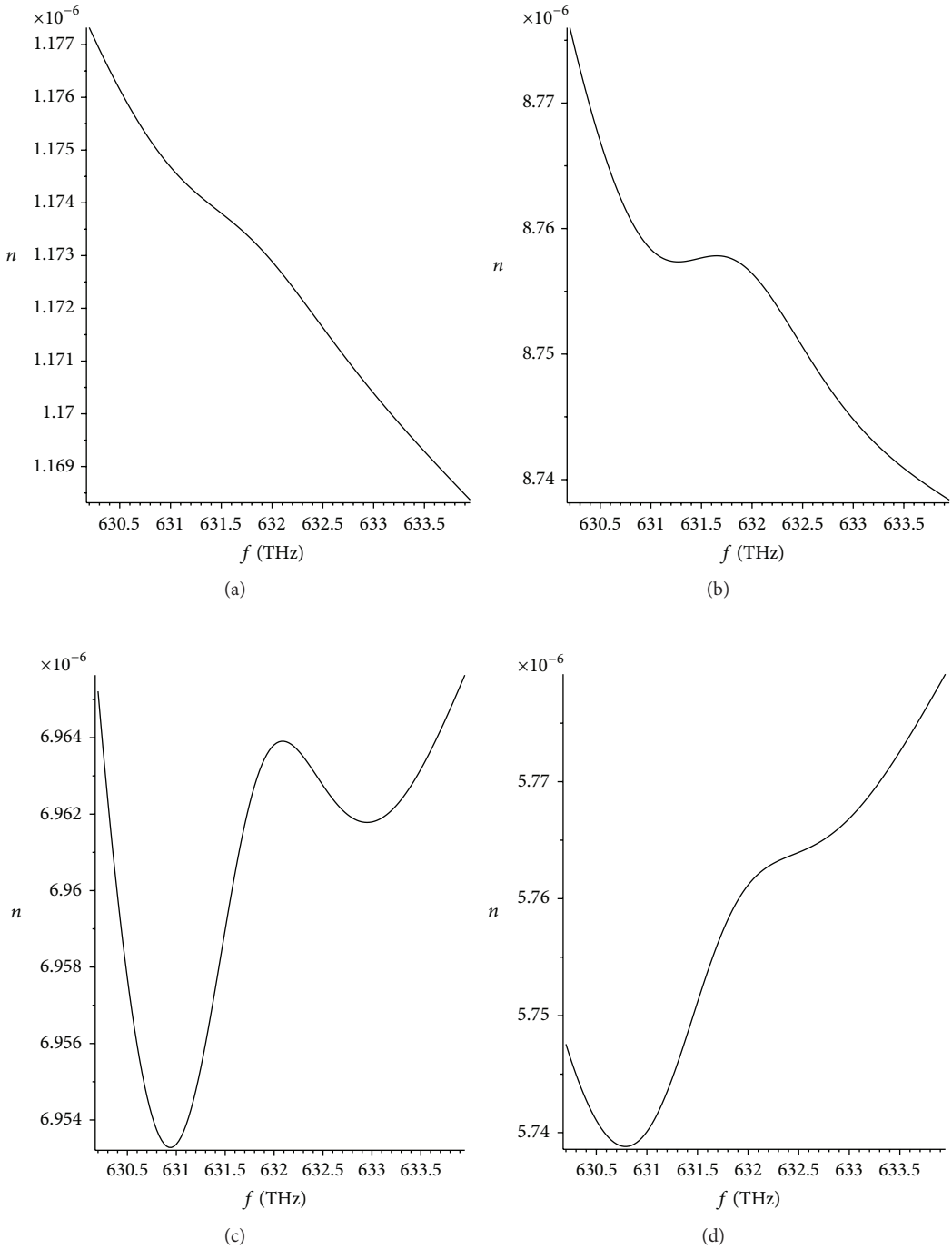

Figure 3: The real part of the effective refractive index, n, versus the frequency for different dielectric core thicknesses. In (a), $t = 30$ nm, (b) 40 nm, (c) 50 nm, and (d) 60 nm.

The real part of the effective refractive index increases with the mode order increase. Despite this increase the structure still holds near-zero effective refractive index values for all modes order. For each mode the effective refractive index variations in the allowed frequency spectrum are very small with negative slope. In Figure 7(b), we plot the imaginary part of the effective refractive index, the extinction coefficient for the same set of modes. The dashed curve for $m = 0$, which shows highest values of the extinction coefficient and other curves decrease as the mode order increase.

In Figure 8(a), we plot the power confinement factor and the power attenuation for the same set of modes. The lowest mode, $m = 0$, has the lowest power confinement, and the highest mode $m = 3$ has the highest power confinement. However, power guiding through this structure is still good enough to be used in a wide variety of applications. In

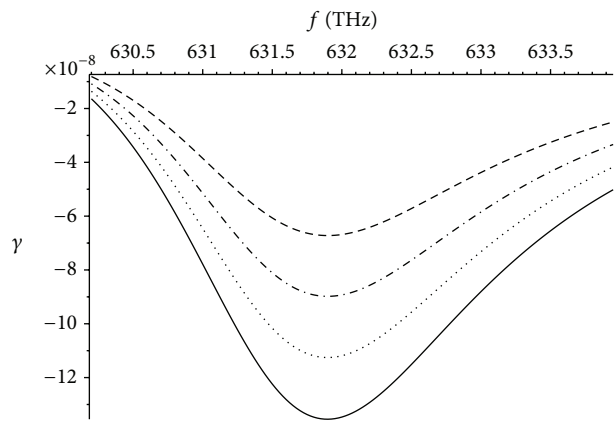

Figure 4: The imaginary part of the effective refractive index (the extinction coefficient), γ, versus the frequency for different dielectric core thicknesses. The core thicknesses are 30 nm (dashed), 40 nm (dot-dashed), 50 nm (dotted), and 60 nm (solid).

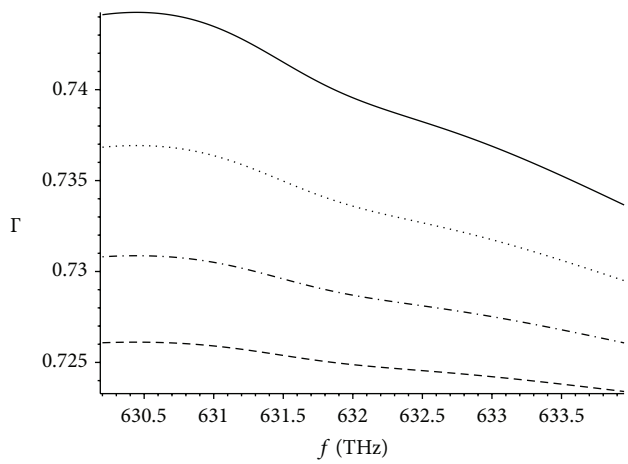

Figure 5: The power confinement factor versus the operating frequency for different dielectric core thicknesses. The core thicknesses are 30 nm (dashed), 40 nm (dot-dashed), 50 nm (dotted), and 60 nm (solid).

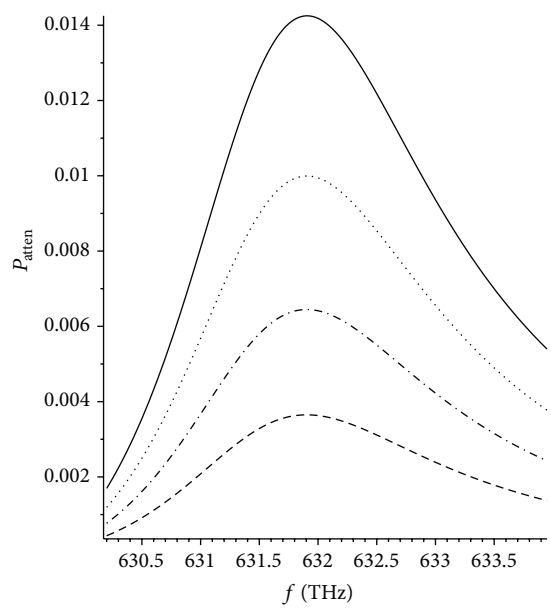

Figure 6: The power attenuation versus the operating frequency for different dielectric core thicknesses. The core thicknesses are 30 nm (dashed), 40 nm (dot-dashed), 50 nm (dotted), and 60 nm (solid).

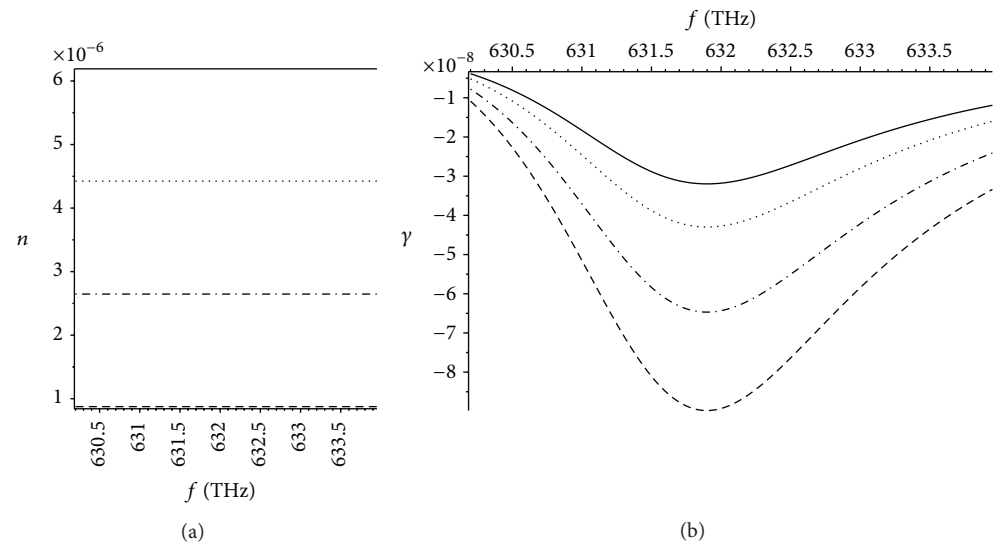

Figure 7: (a) The real part of the effective refractive index, n, versus the frequency for TE_m, $m = 0, 1, 2, 3$. (b) The imaginary part of the effective refractive index (the extinction coefficient), γ, versus the frequency for same set of modes. Note that $m = 0$ (dash), $m = 1$ (dot-dashed), $m = 2$ (dotted), and $m = 3$ (solid).

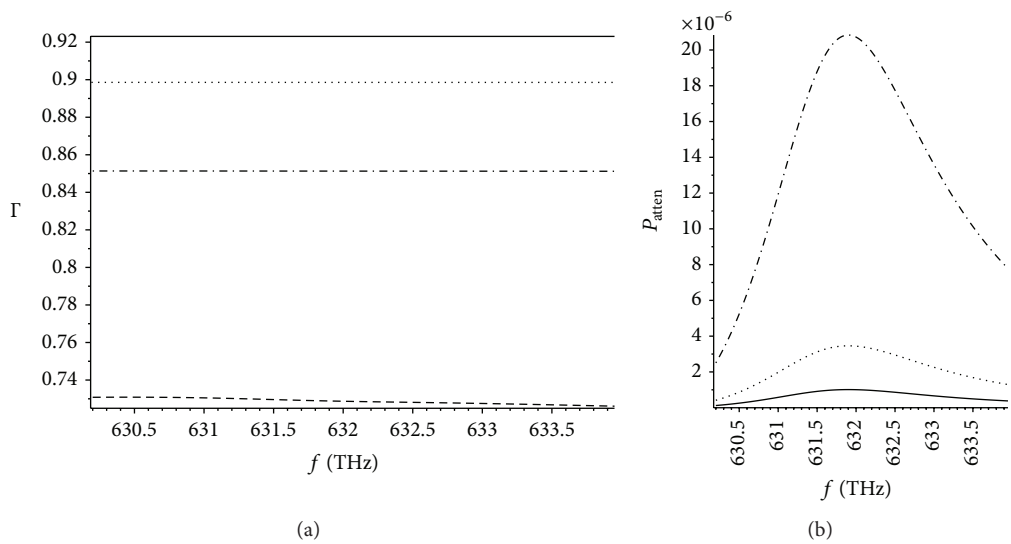

Figure 8: (a) The power confinement factor versus the operating frequency for mode orders $m = 0, 1, 2$, and 3. (b) The power attenuation versus the operating frequency for modes orders $m = 1, 2$, and 3. Note that $m = 0$ (dash), $m = 1$ (dot-dashed), $m = 2$ (dotted), and $m = 3$ (solid).

Figure 8(b), we plot the power attenuation for the first three modes, $m = 1, 2, 3$, and omitted the lowest mode for clarity reasons. The power attenuation decreases with mode order increase, and this attenuation gets the highest values at 632 THz.

5. Conclusion

In this paper, we have used a new class of left-handed materials, which uses 3D nanospheres distributed in loops in the dielectric host material. These 3D nanospheres loops give rise to negative effective permeability and permeability at Terahertz (optical) frequencies. We analytically studied the TE surface waves modes in a slab waveguide at optical frequencies. The structure has a dielectric film (BaF_2) between two thick layers of terahertz left-handed material. A dispersion relation for TE surface waves has been derived and numerically investigated. We found near-zero real effective refractive index for the allowed frequency range and at different dielectric slab thickness and modes orders. Besides that, we found the extinction coefficient of the structure claims small negative values, which means the structure is transparent in the allowed frequency range. The power confinement increases with core's thickness increase and with mode order increase. Besides that the power attenuation claims small values for different core's thicknesses and modes order. This

class of waveguide structure could be used in transmission lines, microstrip resonators, couplers, and antennas.

Acknowledgments

The author of this paper would like to thank Fulbright Scholarship and the Department of Physics at University of Dayton, Ohio, USA, for their support during his research. He would like to thank Professor Leno Pedrotti for helpful and fruitful discussion on the subject. Besides that, He would like to thank Al-Azhar University, Gaza, for their generous support.

References

[1] V. G. Veselago, "The electrodynamics of substances with simultaneously negative values of ε and μ," *Soviet Physics Uspekhi*, vol. 10, pp. 509–514, 1968.

[2] D. R. Smith, W. J. Padilla, D. C. Vier, S. C. Nemat-Nasser, and S. Schultz, "Composite medium with simultaneously negative permeability and permittivity," *Physical Review Letters*, vol. 84, no. 18, pp. 4184–4187, 2000.

[3] R. A. Shelby, D. R. Smith, and S. Schultz, "Experimental verification of a negative index of refraction," *Science*, vol. 292, no. 5514, pp. 77–79, 2001.

[4] B. I. Wu, W. Wang, J. Pacheco, X. Chen, T. Grzegorczyk, and J. A. Kong, "A study of using metamaterials as antenna substrate to ehance Gain," *Progress in Electromagnetics Research*, vol. 51, pp. 295–328, 2005.

[5] H. J. Lezec, J. A. Dionne, and H. A. Atwater, "Negative refraction at visible frequencies," *Science*, vol. 316, no. 5823, pp. 430–432, 2007.

[6] M. Gil, F. Aznar, A. Velez et al., "Electrically small resonators for metamaterial and microwave circuit design," in *Passive Microwave Components and Antennas*, V. Zhurbenko, Ed., InTech, 2010.

[7] J. Qi Shen, "Introduction to the theory of left-handed media," Submitted, http://arxiv.org/abs/cond-mat/0402213.

[8] C. Caloz and T. Itoh, "Application of the transmission line theory of lefthanded (LH) materials to the realization of a microstrip LH transmission line," in *Proceedings of the IEEE AP-S International Symposium and USNC/URSI National Radio Science*, vol. 2, San Antonio, Tex, USA, June 2002.

[9] C. Caloz and T. Itoh, *Electromagnetic Metamaterials: Transmission Line Theory and Microwave Applications*, IEEE Press, New York, NY, USA, 2005.

[10] C. Caloz and T. Itoh, "Transmission line approach of left-handed (LH) materials and microstrip implementation of an artificial LH transmission line," *IEEE Transactions on Antennas and Propagation*, vol. 52, no. 5, pp. 1159–1166, 2004.

[11] C. Caloz and T. Itoh, "A novel mixed conventional microstrip and composite right/lefthanded backward-wave directional coupler with broadband and tight coupling characteristics," *IEEE Microwave and Wireless Components Letters*, vol. 14, no. 1, pp. 31–33, 2004.

[12] S. Otto, A. Rennings, C. Caloz, P. Waldow, I. Wolff, and T. Itoh, "Composite right/lefthanded λ-resonator ring antenna for dual-frequency operation," in *Proceedings of the IEEE AP-S International Symposium and USNC/URSI National Radio Science*, Washington, DC, USA, June 2005.

[13] A. Sanada, M. Kimura, I. Awai, C. Caloz, and T. Itoh, "A planar zeroth-order resonator antenna using a left-handed transmission line," in *Proceedings of the 34th European Microwave Conference*, pp. 1341–1344, Amsterdam, The Netherlands, October 2004.

[14] N. Fang, H. Lee, C. Sun, and X. Zhang, "Sub-diffraction-limited optical imaging with a silver superlens," *Science*, vol. 308, no. 5721, pp. 534–537, 2005.

[15] H. S. Chen, B. I. Wu, B. Zhang, and J. A. Kong, "Electromagnetic wave interactions with a metamaterial cloak," *Physical Review Letters*, vol. 99, no. 6, Article ID 063903, 2007.

[16] C. R. Williams, S. R. Andrews, S. A. Maier, A. I. Fernández-Domínguez, L. Martín-Moreno, and F. J. García-Vidal, "Highly confined guiding of terahertz surface plasmon polaritons on structured metal surfaces," *Nature Photonics*, vol. 2, no. 3, pp. 175–179, 2008.

[17] V. J. Logeeswaran, A. N. Stameroff, M. S. Islam et al., "Switching between positive and negative permeability by photoconductive coupling for modulation of electromagnetic radiation," *Applied Physics A*, vol. 87, no. 2, pp. 209–216, 2007.

[18] J. B. Pendry, A. J. Holden, W. J. Stewart, and I. Youngs, "Extremely low frequency plasmons in metallic mesostructures," *Physical Review Letters*, vol. 76, no. 25, pp. 4773–4776, 1996.

[19] H.-T. Chen, W. J. Padilla, J. M. O. Zide, A. C. Gossard, A. J. Taylor, and R. D. Averitt, "Active terahertz metamaterial devices," *Nature*, vol. 444, no. 7119, pp. 597–600, 2006.

[20] A. Alù, A. Salandrino, and N. Engheta, "Negative effective permeability and left-handed materials at optical frequencies," *Optics Express*, vol. 14, no. 4, pp. 1557–1567, 2006.

[21] J. Yao, Z. Liu, Y. Liu et al., "Optical negative refraction in bulk metamaterials of nanowires," *Science*, vol. 321, no. 5891, p. 930, 2008.

[22] A. Vallecchi and M. Albani, "Negative effective refractive index metamaterials at optical frequencies based on superlattices of noble metals and excitonic semiconductors," in *Proceedings of the 30th URSI General Assembly and Scientific Symposium (URSIGASS '11)*, August 2011.

[23] P. Chaturvedi, *Optical metamaterials: design, characteristics and applications [Ph.D. thesis]*, University of Illinois at Urbana-Champaign, 2009.

[24] R. A. Depine, M. L. Martínez-Ricci, J. A. Monsoriu, E. Silvestre, and P. Andrés, "Zero permeability and zero permittivity band gaps in 1D metamaterial photonic crystals," *Physics Letters A*, vol. 364, no. 3-4, pp. 352–355, 2007.

[25] Y. Xu and H. Chen, "Total reflection and transmission by epsilon-near-zero metamaterials with defects," *Applied Physics Letters*, vol. 98, no. 11, Article ID 113501, 2011.

[26] S. Kocaman, M. S. Aras, P. Hsieh et al., "Zero phase delay in negative-refractive-index photonic crystal superlattices," *Nature Photonics*, vol. 5, no. 8, pp. 499–505, 2011.

[27] E. Vesseur, T. Coenen, H. Caglayan, N. Engheta, and A. Polman, "Experimental verification of $n = 0$ structures for visible light," *Physical Review Letters*, vol. 110, Article ID 013902, 2013.

[28] J. Schilling, "Fundamental optical physics: the quest for zero refractive index," *Nature Photonics*, vol. 5, no. 8, pp. 449–451, 2011.

[29] A. Alù, M. G. Silveirinha, A. Salandrino, and N. Engheta, "Epsilon-near-zero metamaterials and electromagnetic sources: tailoring the radiation phase pattern," *Physical Review B*, vol. 75, no. 15, Article ID 155410, 2007.

[30] X.-X. Liu and A. Alù, "Homogenization of quasi-isotropic metamaterials composed by dense arrays of magnetodielectric spheres," *Metamaterials*, vol. 5, no. 2-3, pp. 56–63, 2011.

[31] D. V. B. Murthy, A. Corona-Chávez, and J. L. Olvera-Cervantes, "A novel Epsilon Near Zero (ENZ) tunneling circuit using microstrip technology for high integrability applications," *Progress In Electromagnetics Research C*, vol. 15, pp. 65–74, 2010.

[32] V. Mocella, S. Cabrini, A. S. P. Chang et al., "Self-collimation of light over millimeter-scale distance in a quasi-zero-average-index metamaterial," *Physical Review Letters*, vol. 102, no. 13, Article ID 133902, 2009.

[33] N. M. Litchinitser, A. I. Maimistov, I. R. Gabitov, R. Z. Sagdeev, and V. M. Shalaev, "Metamaterials: electromagnetic enhancement at zero-index transition," *Optics Letters*, vol. 33, no. 20, pp. 2350–2352, 2008.

[34] R. W. Ziolkowski, "Propagation in and scattering from a matched metamaterial having a zero index of refraction," *Physical Review E*, vol. 70, no. 4, Article ID 046608, 12 pages, 2004.

[35] N. Engheta, "Circuits with light at nanoscales: optical nanocircuits inspired by metamaterials," *Science*, vol. 317, no. 5845, pp. 1698–1702, 2007.

[36] P. Diament, *Wave Transmission and Fiber Optics*, Macmillan, 1990.

[37] A. Ishimaru, S.-W. Lee, Y. Kuga, and V. Jandhyala, "Generalized constitutive relations for metamaterials based on the quasi-static Lorentz theory," *IEEE Transactions on Antennas and Propagation*, vol. 51, no. 10 I, pp. 2550–2557, 2003.

[38] J. D. Jackson, *Classical Electrodyanmics*, John Wiley & Sons, 1998.

[39] C. F. Bohren and D. R. Huffman, *Absorption and Scattering of Light By Small Particles*, John Wiley & Sons, New York, NY, USA, 1983.

[40] S. Tretyakov, *Analytical Modeling in Applied Electromagnetics*, Artech House, 2003.

[41] M. J. Adams, *An Introduction to Optical Waveguides*, John Wiley & Sons, 1981.

[42] K. Okamoto, *Fundamentals of Optical Waveguides*, Elsevier, 2006.

[43] J. Singh, *Optical Properties of Condensed Matter and Applications*, John Wiley & Sons, 2006.

[44] A. I. Ass'ad and H. S. Ashour, "TE magnetostatic surface waves in symmetric dielectric negative permittivity material waveguide," *Advances in Condensed Matter Physics*, vol. 2009, Article ID 867638, 5 pages, 2009.

[45] A. D. Boardman, M. M. Shabat, and R. F. Wallis, "TE waves at an interface between linear gyromagnetic and nonlinear dielectric media," *Journal of Physics D*, vol. 24, no. 10, pp. 1702–1707, 1991.